



Integrating both restoration and regeneration potentials into real-world forest restoration planning: A case study of Hong Kong

He Zhang^a, Calvin K.F. Lee^a, Ying Ki Law^a, Aland H.Y. Chan^b, Jinlong Zhang^c, Stephan W. Gale^c, Alice Hughes^{a,d}, Martha J. Ledger^a, Man Sing Wong^e, Amos P.K. Tai^{f,g}, Billy C.H. Hau^a, Jin Wu^{a,d,*}

^a School of Biological Sciences, The University of Hong Kong, Pokfulam, Hong Kong, China

^b Department of Plant Sciences and Conservation Research Institute, University of Cambridge, Downing Street, Cambridge, CB2 3EA, UK

^c Flora Conservation Department, Kadoorie Farm and Botanic Garden, Hong Kong, China

^d Institute for Climate and Carbon Neutrality, The University of Hong Kong, Hong Kong, China

^e Department of Land Surveying and Geo-Informatics, The Hong Kong Polytechnic University, Hong Kong, China

^f Earth and Environmental Sciences Programme, Faculty of Science, The Chinese University of Hong Kong, Hong Kong, China

^g State Key Laboratory of Agrobiotechnology, and Institute of Environment, Energy and Sustainability, The Chinese University of Hong Kong, Hong Kong, China

ARTICLE INFO

Keywords:

Nature-based solution
restoration
Vegetation restoration potential
Natural regeneration
Multi-temporal airborne LiDAR
Canopy height
Hong Kong

ABSTRACT

Forest restoration is a vital nature-based solution for mitigating climate change and land degradation. To ensure restoration effectiveness, the costs and benefits of alternative restoration strategies (i.e., active restoration vs. natural regeneration) need to be evaluated. Existing studies generally focus on maximum restoration potential, neglecting the recovery potential achievable through natural regeneration processes, leading to incomplete understanding of the true benefits and doubts about the necessity of active restoration. In this study, we introduce a multi-stage framework incorporating both restoration and regeneration potential into prioritized planning for ecosystem restoration. We used the vegetated landscape of Hong Kong (covering 728 km²) as our study system due to its comprehensive fine-resolution data and unique history of vegetation recovery, making it an ideal candidate to demonstrate the importance of this concept and inspire further research. We analyzed vegetation recovery status (i.e., recovering, degrading, and stable) over the past decade based on the canopy height data derived from multi-temporal airborne LiDAR. We assessed natural regeneration potential and maximum restoration potential separately, producing spatially-explicit predictions. Our results show that 44.9% of Hong Kong's vegetated area has showed evidence of recovery, but remaining gains through natural regeneration are limited, constituting around 4% of what could be attained through active restoration. We further estimated restoration priority by maximizing the restoration gain. When prioritizing 5% of degraded areas, the increment in canopy height could be up to 10.9%. Collectively, our findings highlight the importance of integrating both restoration and regeneration potential into restoration planning. The proposed framework can aid policymakers and land managers in optimizing forest restoration options and promoting the protection and recovery of fragile ecosystems.

1. Introduction

Forest restoration is recognized as an effective solution for mitigating climate change, restoring ecosystem services, and protecting biodiversity, offering a wide range of environmental and socio-economic benefits (Griscom et al., 2017, 2020; Lewis et al., 2019). Despite considerable efforts by countries and international organizations to implement large-scale vegetation restoration programs, projects, and plans

(EC-European Commission, 2019; Feng et al., 2016; Mansourian and Berrahmouni, 2021; Messinger and Winterbottom, 2016; Summit, 2014), the demand for restoration remains substantial, with a pledge to restore at least 1 billion hectares of forests by 2050 to help limit global warming to within 1.5 °C (Masson-Delmotte et al., 2018). In addition to sequestering carbon, forest restoration can also contribute to large-scale environmental programs, such as China's Ecological Conservation Redline policy, which focuses on biodiversity and ecosystem services

* Corresponding author. School of Biological Sciences, The University of Hong Kong, Pokfulam, Hong Kong, China.

E-mail address: jinwu@hku.hk (J. Wu).

and urgently requires effective conservation and restoration actions to meet post-2020 protected area targets (Choi et al., 2022). Furthermore, the UN declared 2020 to 2030 as a “Decade on Restoration”, thus understanding how this can be realized most effectively is critical. While acknowledging the importance of forest restoration, it is also essential to understand the ecological limits of forest restoration potential and the socio-economic constraints of different restoration strategies, determining when and where human intervention is necessary for active restoration or natural regeneration (Torrubia et al., 2014).

In recent years, vegetation recovery potential (VRP) has been utilized as an indicator of the peak state of vegetation growth supported by a given biophysical capacity. This concept was initially used to describe the magnitude and distribution of climate mitigation opportunities available through forest restoration on a global scale (Bastin et al., 2019; Walker et al., 2022) and was later adapted to national and regional scales to provide clear restoration goals (Jiang et al., 2022; Meng et al., 2023). Typically, VRP assessment involves coupling data-driven and machine-learning techniques, using undisturbed vegetation to represent the natural carrying capacity of a location. Key metrics (e.g., tree cover or aboveground biomass) of various undisturbed vegetation across large environmental gradients and spatial extents are then assembled and related to geographical and environmental information to help characterize the restoration potential for any given environment worldwide (Bastin et al., 2019; Meng et al., 2023; Walker et al., 2022). Although these findings facilitate the identification of broad trends, patterns and restoration hotspots, they focus solely on maximum restoration potential without adequately considering the extent to which natural regeneration can contribute to the recovery process in a spatially explicit way. This oversight can result in an incomplete understanding of true benefits, costs, and necessity of conducting active restoration in the real-world restoration planning (Chazdon et al., 2021; Crouzeilles et al., 2020).

Compared to active restoration such as planting and seeding, natural regeneration offers a cost-effective approach which can potentially play a major role in large-scale landscape restoration (Chazdon and Uriarte, 2016). Initiated through the colonization of opportunistic and locally adapted species, natural regeneration has the opportunity to result in a higher diversity of native, locally adapted plant species than active tree planting schemes through a stochastic dynamic process (Cook-Patton et al., 2020; Crouzeilles et al., 2017). Unfavorable conditions, however, can impede natural regeneration and push the ecosystem towards an alternate steady state where the diversity, structure, composition or function cannot be fully restored to levels comparable with nearby primary forests. Such impediments can be attributed to local extinctions, severe depletion of local species pools, excessively constrained dispersal capacity due to extirpation of dispersal agents, and arrested succession due to frequent disturbances or environmental barriers such as soil erosion, pathogens, or invasive alien species. This regeneration process can be assisted with human intervention to overcome these limitations, or requiring active restoration under severe conditions using site preparation, tree planting or establishing native tree corridors to facilitate their regrowth through subsequent natural regeneration (Chazdon et al., 2020). In this case, active restoration can act as a complementary measure to accelerate or promote natural regeneration to attain the maximum recovery potential, thereby achieving greater ecological benefits within a given timeframe. As a result, the ecological trajectories achievable by natural regeneration and active restoration can be different. Such disparities in recovery status, rates and potential outcomes exhibit spatial variability across diverse landscapes (Fig. 1), which are rarely evaluated. Consequently, a better understanding and assessment on the status and potential of natural regeneration can provide a basis for more cost-effective restoration planning and landscape management projects that aim to achieve a wide range of long-lasting social and environmental benefits (Chazdon et al., 2021).

In summary, there are three major knowledge gaps in the field which we aim to address: 1) studies focusing on VRPs are primarily conducted

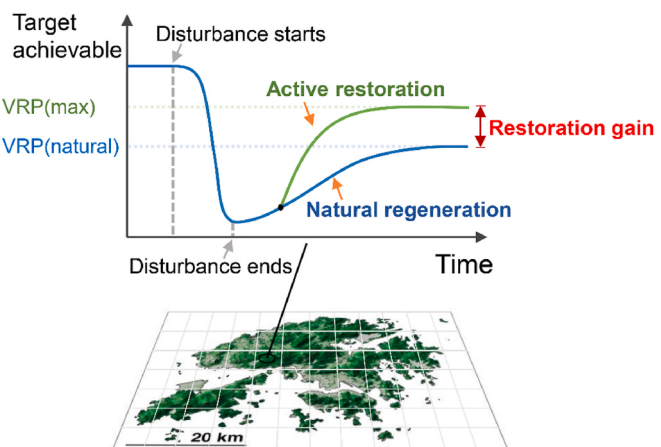


Fig. 1. Conceptual illustration showing an example of recovery trajectory after disturbance within a timeframe where active restoration acts as a complementary measure to accelerate or promote natural regeneration to attain the maximum vegetation restoration potential. The grids on the topographic map represent distinct landscape units, each exhibiting spatial variability in recovery status, rates and potentials, resulting in unique trajectories across landscapes. Figure adapted from Moreno-Mateos et al. (2017).

at coarse spatial resolutions, leading to mismatches with real-world ecosystem restoration practices, particularly in fine-scale planning scenarios; 2) natural regeneration, as a cost-effective means of ecosystem recovery, has not received sufficient attention in most current restoration projects, resulting in inadequate consideration or evaluation of VRP achievable through natural regeneration; and 3) the gaps between natural regeneration potential and maximum restoration potential, as well as their spatial variabilities and trajectories, require better characterization to assess the extent to which natural regeneration approaches can support effective restoration planning.

To address these knowledge gaps, we explore a multi-stage framework, which integrates both maximum restoration and natural regeneration potentials into practical ecosystem restoration planning. This is followed by a case study conducted in Hong Kong to demonstrate its local implementation. We selected Hong Kong as our study system due to the comprehensive data availability and unique history of vegetation recovery, making it an ideal candidate to demonstrate the significance of this concept. Our study helps reveal the key underlying biophysical factors that influence the recovery potentials, and the proposed framework hold the promise of assisting policymakers and landscape managers in optimizing vegetation restoration strategies at flexible scales, ultimately promoting the protection and recovery of degraded ecosystems.

2. Materials and methods

2.1. Overview of the framework

We developed a general framework aiming to quantitatively assess vegetation recovery potentials (VRPs) for efficient restoration planning using multi-temporal remote sensing data in a spatially explicit manner. Notably, VRPs achieved through the two pathways (natural regeneration with or without active intervention) would be distinguished: VRP (natural), i.e., natural regeneration potential, represents the achievable outcome by natural vegetation regeneration without active intervention (Crouzeilles et al., 2020); VRP(max), i.e., maximum restoration potential, signifies the upper limit that an ecosystem can reach in the future with the growth over an infinite timeline, representing the attainable outcome under local biophysical capacity (Bastin et al., 2019; Zuo et al., 2023). The two types of VRPs would be estimated separately with geospatial details, and the differences between the two VRPs serves as a

crucial factor in determining practical restoration priorities and strategies (Fig. 1).

2.2. Study area

Hong Kong Special Administrative Region of China ($22^{\circ}27'35''\text{N}$, $114^{\circ}06'13''\text{E}$) is situated in a sub-tropical monsoon climate, with a mean annual temperature of 23.5°C and mean annual precipitation of 2431 mm (Hong Kong Observatory, <https://www.hko.gov.hk/>). The land area spans 1108 km^2 , with 40% of the land designated as Country Parks or nature reserves.

Hong Kong exhibits a unique history of vegetation recovery with intensive influence of human activities, making it an ideal case study on understanding dimensions of regeneration and restoration. The region's forests had almost entirely been cleared by the late 17th century, with extensive attempts in reforestation and the subsequent establishment of the Country Park system after World War II (Zhuang and Gorlett, 1997). However, this process has frequently been disturbed by human-induced hill fires and other natural hazards, resulting in a strong disturbance gradient comprising a mosaic of grassland, shrubland, evergreen secondary forests, and old-growth *feng shui* woodland that have been protected from deforestation for centuries, with artificially reinforced ecological boundaries between them. Consequently, variation in recovery status, rates, and potentials across these landscapes enable us to better understand the underlying biophysical factors shaping landscape disparities. Second, Hong Kong offers a wealth of high-resolution data that is critical for informing practical restoration planning. This data is particularly useful in making accurate assessments of real-world forest recovery status and providing detailed, spatially explicit information. Over the years, the Hong Kong government has collected multi-temporal airborne LiDAR data for the entire city, providing invaluable forest structure information. Additionally, annual aerial photographs of the city have been collected since the 1960s, allowing for the identification of vegetation type history across the city. Furthermore, fine-scale grid-based environmental datasets are available in Hong Kong for use in this study, including data on climate, topography and soil (Luo et al., 2007; Morgan and Guénard, 2018, 2019).

2.3. Materials

We utilized multi-source remote sensing data in this study, including airborne LiDAR data, historical aerial photographs, and 30-m resolution climate, topography and soil datasets.

(1) Airborne LiDAR data

The airborne LiDAR data includes vegetation structural data and terrain data. The surveys, commissioned by the Geotechnical Engineering Office of the Civil Engineering and Development Department (CEDD), covered all territories of Hong Kong and were conducted in 2010 and 2020, respectively. We pre-processed the raw point cloud by denoising, filtering, and normalization using LAStools (Isenburg, 2020). Notably, filtering steps classified ground points, and a 5-m resolution digital terrain model (DTM) was interpolated using the ordinary kriging method (Zhao et al., 2016); the normalization step removed the influence of terrain elevation on LiDAR point clouds by subtracting the DTM value from the original point height at the corresponding location. Based on the normalized LiDAR point clouds, a canopy height model (CHM) was produced, from which we calculated mean top-of-canopy height (TCH), as the mean height of pixels composing the CHM surface.

(2) Environmental data

We used a published high-resolution dataset to describe the environmental conditions of the study region. This dataset comprises 30-m resolution raster GIS layers for Hong Kong's terrestrial environments,

including climate, vegetation, topography, and urban development (Morgan and Guénard, 2019). We expanded this archive with soil properties at surface layer, including soil cation exchange capacity (CEC), soil organic carbon (SOC), Nitrogen (N) and Phosphorus (P) contents (Luo et al., 2007). This dataset was input into the predictive model as predictors to estimate the maximum VRP constrained by environmental conditions. Detailed variables are available in Table A1.

(3) Historical aerial photos

The historical aerial photograph dataset provided historical land-use information for Hong Kong. The surveys were conducted by the Lands Department on an approximately annual basis between 1964 and mid-2016. Due to the extensive efforts required in data downloading, mosaicking, georeferencing, and other pre-processing, we only used the data covering the entire Hong Kong on appropriately 10-year intervals from the mid-1960s, including images from 1964, 1973, 1982, 1990, 1999 and 2010. The resolution is approximately 0.1 m in greyscale (except for 2010 which is in RGB). The aerial photos were georeferenced using OpenStreetMap. This dataset enabled us to: 1) identify disturbed areas (e.g., landslides) by manually delineating regions affected by landslide disturbances; and 2) provide external validation for assessing the accuracy of the estimated VRPs.

(4) Disturbance mapping

We included two disturbance layers (fires and landslides). The fire maps were generated using a Landsat-based burn-area time series, where the burn areas in Hong Kong were mapped across a 35-year Landsat multispectral time series (1986–2020) using a LTSfire pipeline (Chan et al., 2023). The landslide maps were generated from aerial photos by manual delineation (Law et al., accepted). These layers help to identify VRP under natural regeneration scenario in the absence of disturbances.

2.4. Methods

The four key steps outlined below adheres to the overview of our proposed multi-stage framework introduced in Section 2.1, as shown in Fig. 2. Firstly, we assessed the present-day vegetation recovery status (recovering, degrading or stable) to serve as baseline information. We then identified and differentiated VRP(natural) and VRP(max) from existing patches for estimating their values. Next, we mapped the two types of VRPs for the entire region using spatial interpolation and predictive modeling, based on geographical proximity (Chazdon, 2013) and environmental similarity (Bastin et al., 2019). Finally, we used these results to determine prioritized restoration plans based on the estimated restoration gain. Detailed procedures are described below.

(1) Characterizing recovery status

In this case study, we used canopy height as a demonstration indicator of VRPs for the following reasons: i) canopy height is an easy-to-measure index that can be derived from various LiDAR-based products with high accessibility, extensive coverage, and low computational cost; ii) unlike spectral-based indices (such as NDVI or tree cover), structural indices are less susceptible to the saturation effect, particularly in tropical regions with dense tree canopies (Phillips et al., 2008); and iii) there is a strong correlation between canopy height and aboveground biomass, as well as species composition and other ecological functions (Cazzolla Gatti et al., 2017; Gamfeldt et al., 2013), suggesting that canopy height serves as a starting metric to demonstrate and evaluate this theoretical framework. It should be noted that, one single indicator would have limitations for a holistic assessment on ecological recovery, e.g., canopy height may not adequately reflect the growth of understory and tree recruitment. Therefore, we suggest including more Essential

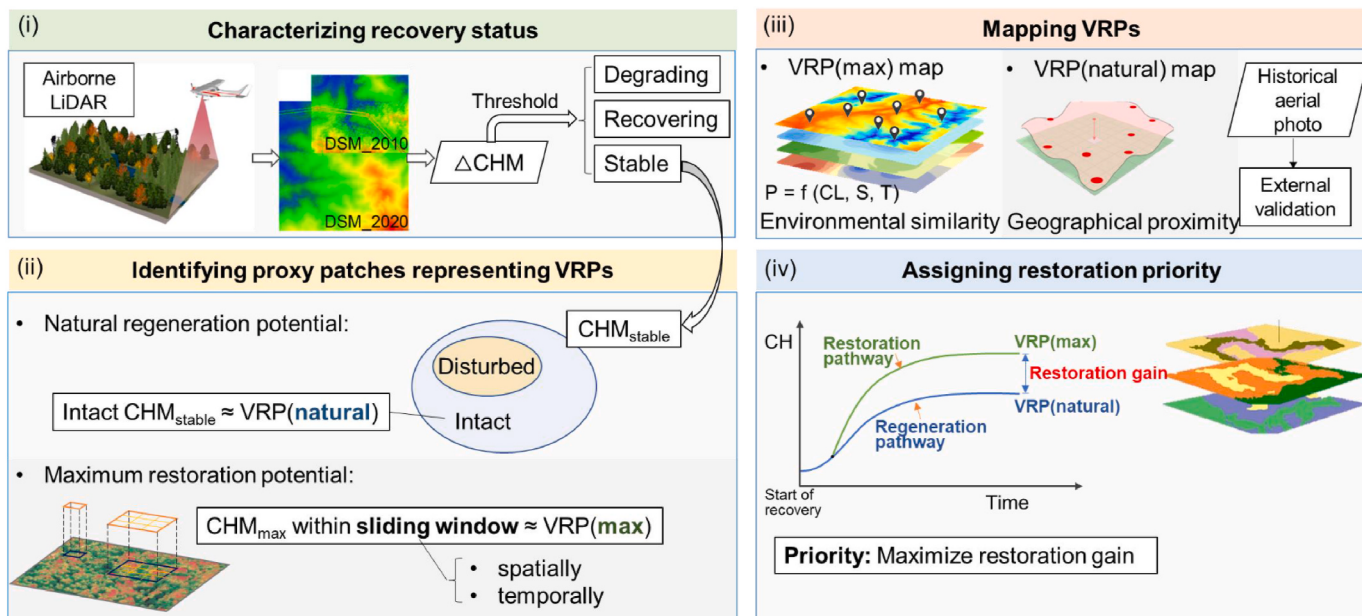


Fig. 2. Methodology flow chart showing the framework of using remote sensing and integrated date-driven approaches to characterize vegetation recovery status and estimate VRPs.

Biodiversity Variables (EBVs; Pereira et al., 2013) in follow-up studies.

We used the canopy height models (CHM) derived from airborne LiDAR data to characterize vegetation recovery status over the past decade in the Hong Kong region. Specifically, we excluded non-vegetated regions by using a land utilization mask developed by the

Planning Department of Hong Kong (https://www.pland.gov.hk/pla_nd_en/info_serv/open_data/landu/). The CHM data from 2010 to 2020 were compared to detect height changes in vegetation, with the difference in CHM between the two time periods calculated pixel by pixel to produce a change map over the decade. Based on the height change, we

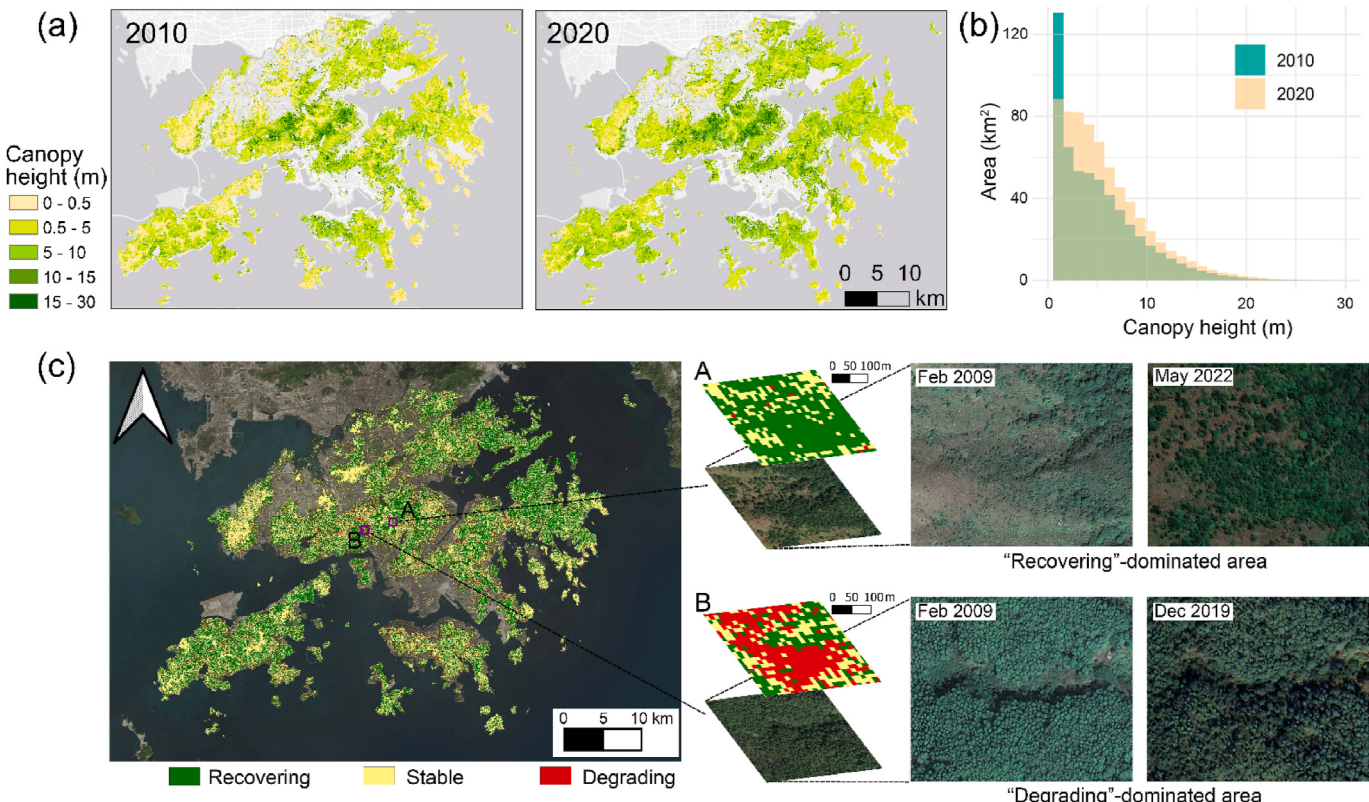


Fig. 3. Vegetation recovery status in Hong Kong from 2010 to 2020. (a) Canopy height maps for 2010 and 2020. (b) Distribution of canopy height extent from 2010 to 2020. Note: the color scheme distinguishes histograms of the two separate years, with blue representing the year 2010, orange representing the year 2020, and pink representing the overlap. (c) Recovery status map featuring example hotspots of “Recovering”-dominated area and “Degrading”-dominated area using 15% of CH_{max} (maximum value of the canopy height in 2010 and 2020) as the threshold.

characterized the vegetation recovery status into (1) recovering, (2) degrading, (3) stable. In doing so, we adopted a threshold approach to characterize the relative canopy height change between 2010 and 2020. We tested a range of thresholds based on the percentage of the baseline height (maximum canopy height during each grid's period) using a sensitivity test (Fig. A1). To prevent the characterization of short vegetation areas from being overly sensitive due to a low threshold, we limited an absolute threshold of 0.5 m, which aligns with the maximum height typically observed in most grassland species (van Jersel et al., 2018). Meanwhile, by cross-comparing the sample plots with known vegetation recovery status (e.g., recent disturbance sites, old intact fengshui wood, and historical restoration sites) through visual evaluation, we chose a 15% change as the threshold value as it could best separate all different recovery statuses in our data records (as shown in Fig. 3c). Following this threshold, if the absolute change in vegetation height exceeded this threshold, the vegetation was considered as recovering or degrading in this area; otherwise, the area was deemed stable.

(2) Identifying proxy patches for estimating VRPs

We identified areas that have reached their VRPs to serve as proxy patches for estimating and mapping VRPs across boarder areas.

The proxy patches for VRP(natural) were determined using stable regions identified in the previous step. We recognize that stable canopy heights may result from vegetative growth being balanced out by disturbances rather than sites reaching their VRPs, so we excluded areas that experienced fires and landslides since 2010. The remaining regions identified as “intact stable” were considered to be representative of areas that have achieved their natural regeneration potential.

The proxy patches for VRP(max) were determined using a sliding-window approach, which selects the maximum vegetation height achieved within a geographically proximate area. For a given location (i,j) in the canopy height raster, the maximum canopy height (CH_{max}) within a sliding window of size w is:

$$CH_{max_w}(i,j) = \max\{CH(x,y) | x, y \in w(i,j)\} \quad (1)$$

Where $CH(x,y)$ is the canopy height at location (x,y) and $w(i,j)$ is the moving window centered at location (i,j) with a window size w .

Then, the standard deviation (SD) between the maximum heights at location (i,j) when using different window sizes is:

$$SD(i,j) = StdDev\{CH_{w1}(i,j), CH_{w2}(i,j), \dots, CH_{wn}(i,j)\} \quad (2)$$

Where $CH_{w1}(i,j)$, $CH_{w2}(i,j)$, ..., $CH_{wn}(i,j)$ are the maximum heights at location (i,j) calculated using different window sizes w_1 , w_2 , ..., w_n , and $StdDev$ is the standard deviation function.

Areas with low SD exhibit a higher likelihood of attaining the maximum canopy height within their specific environmental conditions. The underlying assumption is that if the variation in maximum vegetation height across varying sizes of sliding windows is low, the VRP (max) at that location, constrained by ambient environmental factors, is more likely to fall within that range. The determination of SD threshold considers the trade-off between available sample amounts and confidence level (i.e., how possible the samples can accurately reflect the characteristics of maximum canopy height). In this context, we opted for the first quartile of the sorted SD, selecting the grids as sample points where the SD is below this threshold (Fig. A2). While some subjectivity may be present, this choice ensures a balance between sample size, distribution and confidence level, as shown in Fig. A2. The setting of the sliding window size w considered two aspects: 1) For the convenience of data processing, it is set as integer multiple of the resolution of main remote sensing products (30 m); 2) Considering the seed dispersal distance for woodland species (Heydel et al., 2014), we used 1 km as the maximum w , and included the following sizes: 30, 60, 120, 240, 480, and 960 m.

(3) Mapping VRPs

Spatially continuous VRP maps were subsequently generated based on the proxy patches.

For VRP(natural), since natural regeneration is driven by the colonization of local species, we estimated it based on geographical proximity, employing kriging interpolation that leverages the spatial autocorrelation inherent in the known data (i.e., “intact stable” patches) to estimate values at unmeasured locations (Cressie, 1990). Meanwhile, we also estimated the spatially-explicit uncertainty for the interpolation.

For VRP(max), we assume that environmental conditions constrain the maximum restoration potential. Therefore, we employed a Random Forest model to relate the grid-level VRP(max) determined above to wall-to-wall environmental variables (Table A1). A subset of 50,000 observations was randomly selected from the proxy patches containing the predictor variables, and collinear variables were removed using a correlation threshold of 0.7 (Dormann et al., 2013). We used 70% of the observations for training the model and the remaining 30% for validation. The generalized predictive model takes the form of:

$$VRP(max) = f(V_1, V_2, \dots, V_n) \quad (3)$$

Where VRP is a function of predictor variable classes, and V_1, V_2, \dots, V_n represent the environmental variables.

The model was assessed using root mean square error (RMSE) and coefficient of determination (R^2). To identify variable importance and understand their impacts, we employed the “importance” function from the randomForest package in R, which computed the relative significance of predictor variables in a random forest model. Additionally, we used partial dependence plots for the important variables to gain insights into how they influence the response variable (Greenwell, 2017).

After generating the VRP maps, we used historical aerial photographs to verify our results. From these photographs, we created a dataset containing 8575 polygons by visually interpreting their land cover types (i.e., forest, shrubland, and grassland). This data mapped out the historical presence of forest cover, which provided additional verification for the predicted VRPs. We assume the presence of forest in the past decades corresponds to a potential canopy height of 5 m or above, following previous studies defining tropical trees/forests (Potapov et al., 2022). Accordingly, we calculated the percent agreement of the matching grid numbers between our VRP predictions (≥ 5 m) and historical forest cover (recorded at least once). This consistency serves as an independent verification on the accuracy of our VRP estimates.

(4) Assigning restoration priority

To integrate both restoration and regeneration potentials into practical restoration planning, we proposed a simplified criterion for assigning restoration priority. Specifically, we define the restoration gain as the gap between VRP(max) and VRP(natural). By identifying the top percentiles of this gap, we can locate the areas that urgently need vegetation restoration and are most effective for such restoration efforts. For demonstration, we highlighted the areas with top 5%, 10% and 20% of the restoration gain.

3. Results

3.1. Recovery of Hong Kong vegetation over the past decade

The comparison of canopy height models between 2010 and 2020 reveals a general trend of vegetation recovery in Hong Kong over the past decade (Fig. 3a). This is particularly evident in two ways: 1) the area occupied by vegetation below 1 m height has noticeably decreased (ca. 42 km^2); and 2) vegetation above 1 m height has increased across all height categories (Fig. 3b). This demonstrates substantial vegetation recovery in the area. The spatial distribution of the recovery status can

be found in Fig. 3c. The maps show that higher canopy heights are not evenly distributed but are more concentrated towards the center of the forested areas, which could be due to edge effects where the forest edges (typically lower canopy heights) are more susceptible to environmental changes and human-induced disturbance. Our sensitivity analysis demonstrates that the proportion of recovering/degrading areas remains relatively stable (4.2–4.5 times) within a range of threshold value (i.e., 5%–30%; Fig. A1), indicating that our generated vegetation recovery status is reasonably accurate. Due to its relative insensitivity, we used a threshold of 15% of the baseline height for illustration. Among all three recovery statuses, the recovering area amounts to 326.6 km², constituting 44.9% of Hong Kong's total vegetation area, the stable area encompasses 328.5 km², while the degrading area occupies 72.8 km². Collectively, our results demonstrate that a large proportion of Hong Kong's vegetation is recovering over the past decade.

3.2. Spatial patterns of VRP(natural)

Disturbed areas between 2010 and 2020 were predominantly distributed in the northwest mountainous region of Hong Kong, covering a total of 75.85 km², which accounts for ca. 6.8% of the total land area (Fig. 4a). In contrast to the disturbance pattern, the stable

grids (=VRP(natural)) were found to be widely distributed across Hong Kong, although the canopy height values of these stable grids varied considerably across the landscape. Based on the canopy height values of these stable grids in Fig. 4a, we further developed a model using kriging interpolation to extend the grid level VRP(natural) to the entire Hong Kong, and the model results indicate strong spatial autocorrelation with a RMSE of 0.85 (Fig. 4b). The semivariogram result showed a rising curve that eventually levels off, indicating that points closer to each other (with shorter lag distances) have more similar values of VRP(natural) than points further apart. The estimated range is 2.4 km, beyond which the VRP(natural) is no longer spatially autocorrelated. The associated model-predicted map of VRP(natural) is presented in Fig. 4c, wherein the central mountainous region exhibits higher potential, while the eastern and western coastal areas show lower potential. The southwest region exhibits higher variability in VRP(natural).

3.3. Spatial patterns of VRP(max)

Next, we integrated the derived grid-level VRP(max) (see Methods) with environmental variables and the RF model to estimate and map VRP(max) across the entire Hong Kong. Our results demonstrate high predictive capabilities for VRP(max), with R^2 of 0.67 and RMSE of 2.83

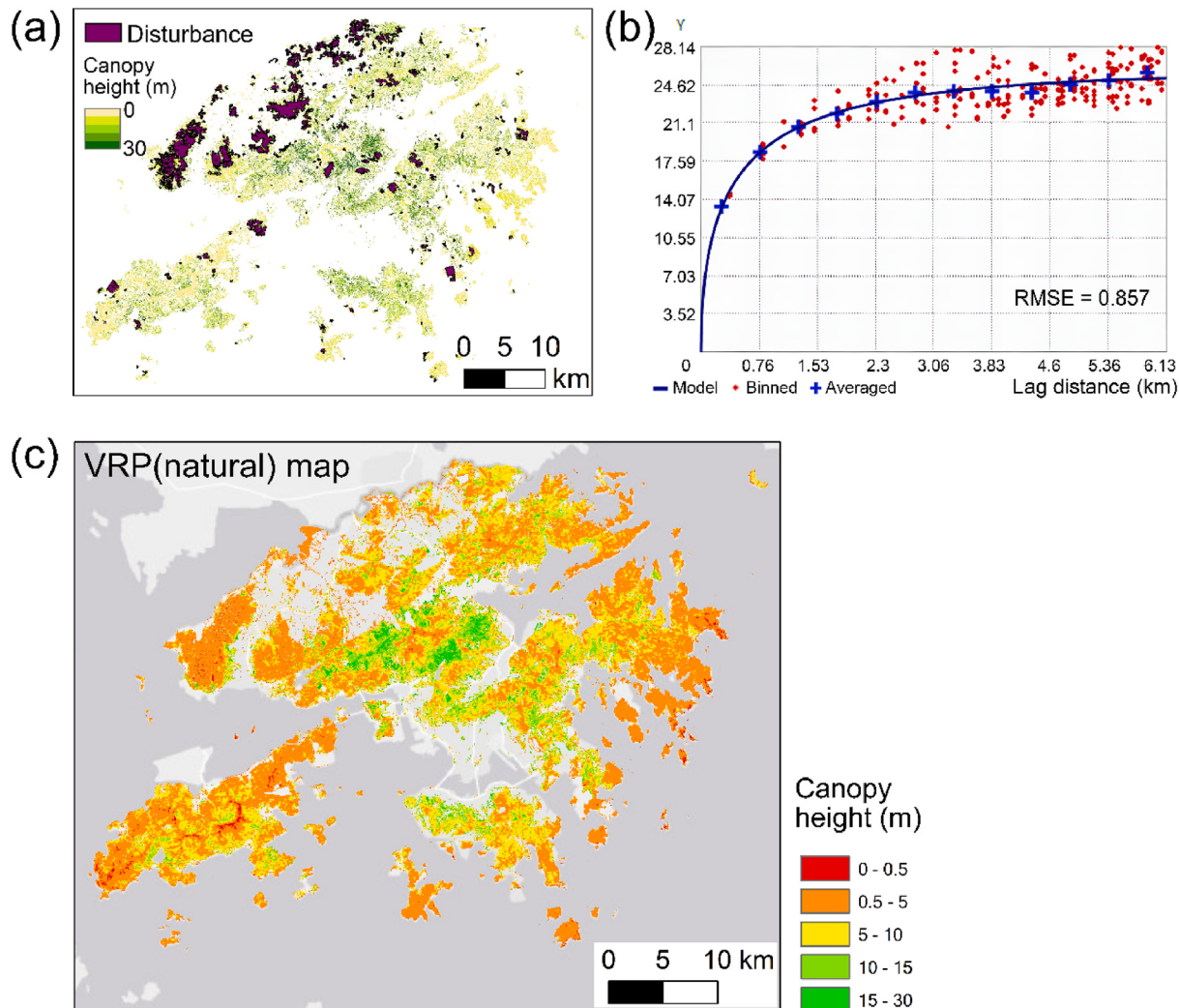


Fig. 4. (a) Distribution of disturbance (fire and landslide) events between 2010 and 2020. The background layer shows the vegetation characterized as “stable” status. (b) Semivariogram showing the spatial autocorrelation in vegetation regeneration. Both the red dots and the blue crosses show the result of binning empirical semivariances, where the binning is done in different ways: the red dots are binned from square cells, and the blue crosses are binned from angular sectors. Details can be found in Gribov et al. (2006). (c) Map of VRP(natural).

m (Fig. 5a). The RF model also attributed relative variable importance, among which the precipitation of warmest quarter (biovars_t18) was identified as the most important variable. Meanwhile, the RF model identified the other three most important variables, i.e., the distance to coast, annual mean relative humidity, and precipitation seasonality (biovars_t15), which together with precipitation of warmest quarter (biovars_t18), accumulatively explained more than 50% of the variation of VRP(max). Since all these variables are directly or indirectly related with plant-available water, this result further indicates that plant water availability is an essential process in determining the natural carrying capacity, thus significantly affecting VRP(max). The corresponding model-predicted map of VRP(max) is presented in Fig. 5c, which again shows a similar pattern as VRP(natural) but with much higher canopy height values compared with VRP(natural).

To further understand the variables' effect on regulating VRP(max), we used partial dependence plots that showcase the average effect of precipitation and the distance to coast on VRP(max) (Fig. A3). The result shows that the VRP(max) is sensitive to precipitation within the range between 800 and 1200 mm yr⁻¹; however, it no longer restricts VRP(max) if precipitation exceeds 1200 mm yr⁻¹ (Fig. A3). In addition, proximity to the coast also constrains VRP(max). Finally, the estimated

maps of VRPs, including both VRP(natural) and VRP(max), were verified using historical aerial photo (Fig. A5) with satisfying consistency, i.e., 76% for VRP(natural) and 91% for VRP(max).

3.4. Restoration priority based on current and VRP maps

The maps of current canopy heights, VRP(natural), and VRP(max) in the Hong Kong region are presented in Fig. A4, and the gaps (i.e., potential-current) for both VRP(natural) and VRP(max) are displayed as histograms in Fig. 6. The results indicate that the current vegetation height closely approximates the estimated VRP(natural), thereby limiting the space for spontaneous natural recovery, constituting around 4% of what could be attained through active restoration, where notable disparity exists between the current vegetation height and VRP(max). This suggests the need for prioritizing active restoration strategies to achieve more substantial rehabilitation results in the future.

To determine the restoration priority, we analyzed the relationship between the gaps of VRP(natural) and VRP(max) (Fig. 7). According to the criteria we have established, restoration priority is assigned to areas that exhibit VRP(max) values significantly higher than VRP(natural), i.e., with maximized restoration gain. Overall, the area classified with top

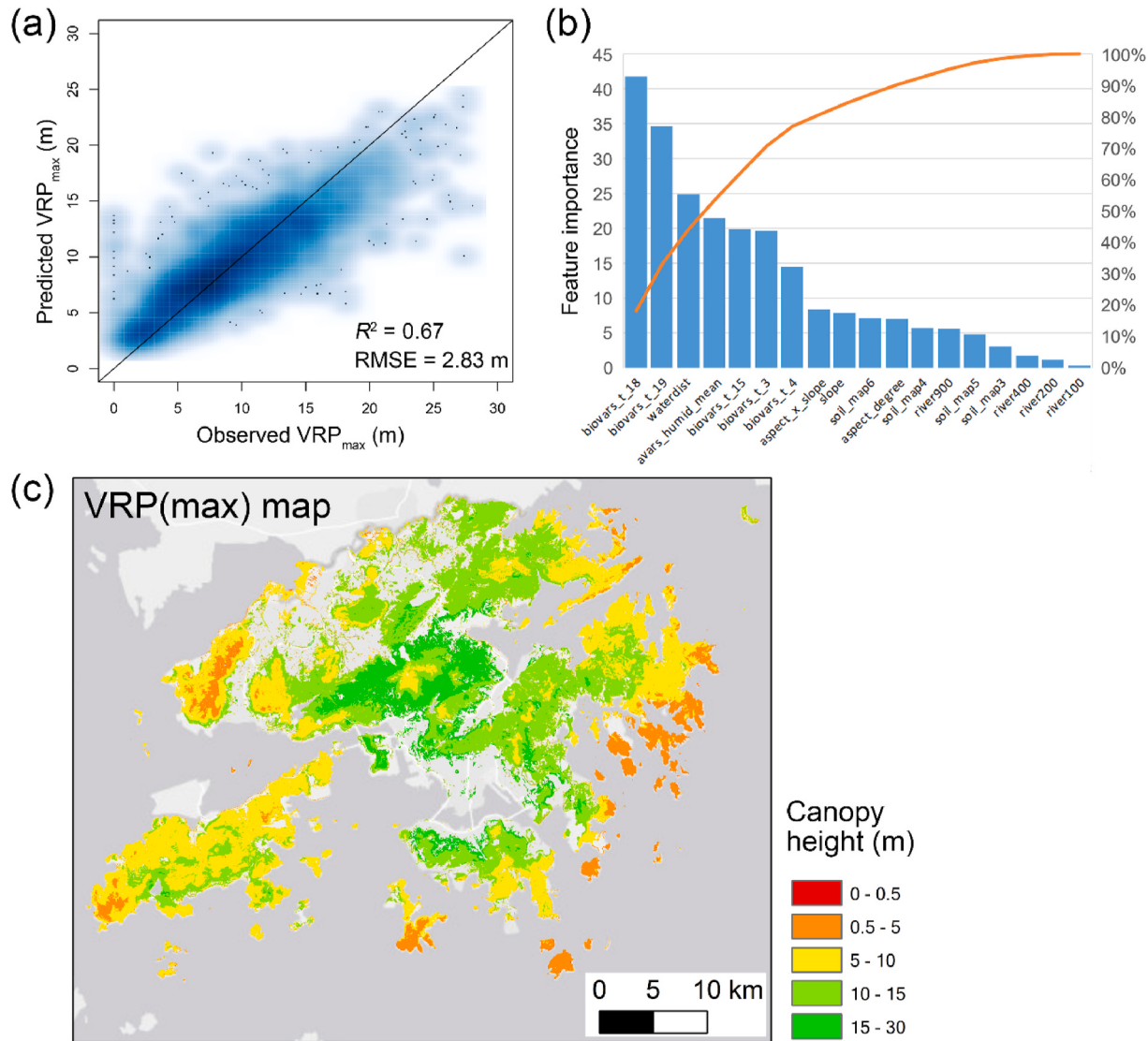


Fig. 5. (a) Observed and predicted VRP(max). (b) Importance of features in the RF regression model. The top three most important variables are: precipitation of warmest quarter (biovars_t18), precipitation of coldest quarter (biovars_t19), and distance to coast (waterdist). Full descriptions of the remaining variables can be found in Supplement (Table A1). (c) Map of VRP(max).

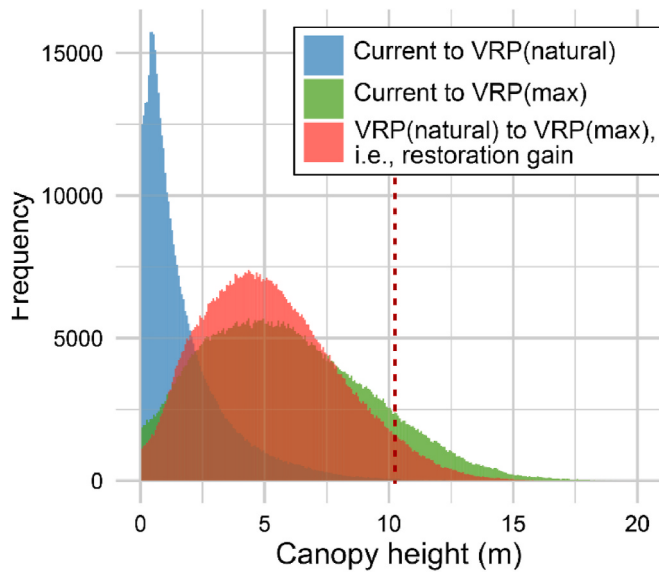


Fig. 6. Histogram showing the gaps between current vegetation height, VRP(natural) and VRP(max) height. The red dash line indicates the threshold for top 5% percentile of restoration gain by area.

5% restoration gain (threshold = 10.23 m) is approximately 3.41 km², accounting for approximately 10.9% of the restoration gain of vegetation height (Fig. 7).

4. Discussion

4.1. Significance of the framework

We devised a multi-stage framework characterizing vegetation recovery status and assessing recovery potentials, allowing for restoration prioritization at a fine spatial scale. Specifically, we emphasized the role of natural regeneration during the recovery process and incorporated both natural regeneration and active restoration into the restoration planning framework. While there is an ongoing debate regarding the superiority of natural recovery over active restoration (Crouzeilles et al., 2017; Reid et al., 2018; H. Zhu et al., 2023), natural regeneration holds significant values as a viable approach for large-scale recovery due to the negligible cost. However, the ability to recover the ecological

function may vary considerably, especially in areas proximate to or isolated from mature forest communities (Chazdon and Guariguata, 2016). The main innovation of our framework is to provide quantitative assessments of the natural regeneration potential and the maximum restoration potential, respectively. This offers a more practical approach when devising vegetation restoration measures, thereby reducing uncertainty and enabling a better grasp of, and reliance on, the outcomes of natural regeneration. In doing so, policymakers and landscape managers can concurrently maximize the overall effectiveness of restoration through natural regeneration while minimizing the necessity for active interventions and their associated costs.

We used Hong Kong to demonstrate that project-level planning with detailed local datasets can distinguish between natural and active recovery in terms of driving factors and potential outcomes. Although this case study relies heavily on remote sensing data with limited integration of field-based information, as input data becomes more diverse and comprehensive, the proposed framework can also be progressively expanded upon, leading to more efficient and accurate formulation of restoration planning. Moreover, this framework demonstrates the potential for scaling up, contributing to ambitious restoration goals at national and global scales. Building upon this foundation, this framework can be further adapted to other aspects of ecosystem functions or services, such as carbon sequestration and species richness (Chazdon, 2013; Poorter et al., 2016). With the continued development in the field of the geographical biology and the increasing availability of big earth data, more and more relevant data will become accessible in the future, and this will facilitate broader applications under the restoration planning concept. Overall, the framework not only facilitates efficient restoration planning but also provides essential baseline data for more accurate predictions of future climate change scenarios using biosphere models.

4.2. Implication of the case study

The case study demonstrates a simple, flexible, and transparent framework to integrate vegetation recovery potentials into restoration planning. Regarding the methodology, we employed two different approaches, geographical proximity and environmental similarity, to separately estimate the natural and maximum vegetation recovery potentials. This differentiation takes into account the distinct mechanisms underlying the two forms of recovery potential. For VRP(natural), natural regeneration is regarded as being driven by the colonization of opportunistic and locally adapted species, where local availabilities of

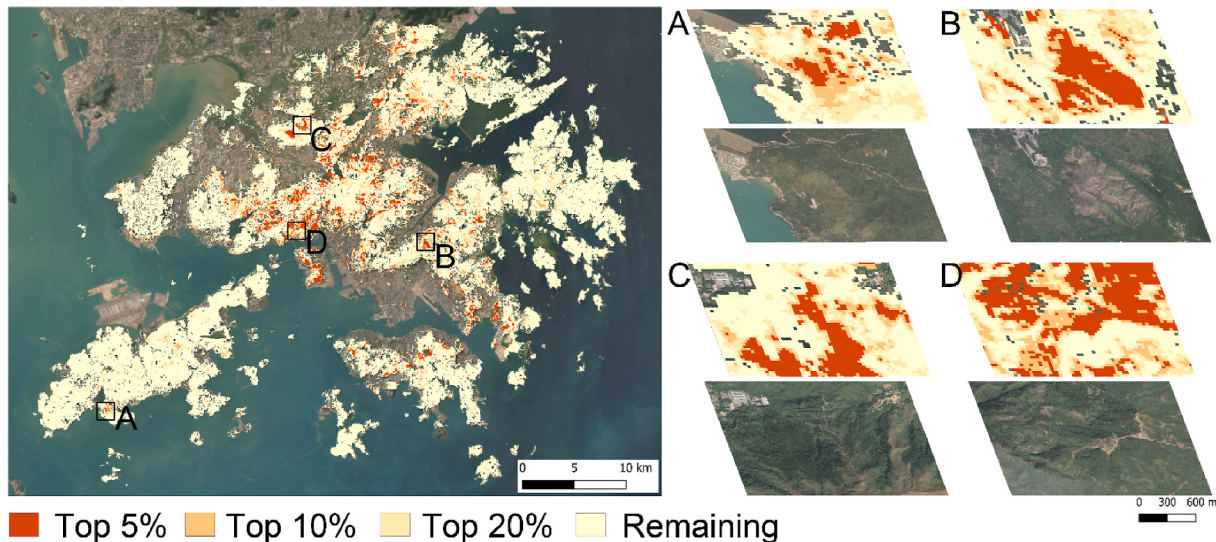


Fig. 7. Restoration priority map with example hotspots. The highlighted areas are with top 5%, 10% and 20% of the restoration gain, respectively.

soil and seeds are highly relevant to this process (Arroyo-Rodríguez et al., 2017). Factors such as residual vegetation providing roosting sites for seed-dispersers (Zahawi et al., 2013) or shade for late-successional species (Ashton et al., 2014) are also associated with the outcomes of natural regenerations. Using spatial interpolation approaches, without restriction to specific data inputs, the underlying influence of these factors can be roughly estimated using spatial autocorrelation. In our case, the semivariogram result has shown that points closer to each other have more similar values (e.g., VRP(natural) under seed dispersal) than points further apart. We determined a range limit of 2.4 km; at distances greater than this, there is a noticeable decline in spatial correlation. This decline suggests a reduced probability for seedlings to establish themselves successfully, originating from a shared seed source. This finding aligns with prior studies on the expected range of seed dispersal in forests as documented by Heydel et al. (2014). Nonetheless, the specific effects of real-world factors are subject to variation across different environmental contexts and species, as well as socioeconomics constrains. When estimating regeneration potential on a larger scale where socioeconomic variables exhibit differentiation, we suggest adopting the method used by Crouzeilles et al. (2020). Their model correlates environmental, climatic, and socioeconomic variables with the occurrence of natural regeneration, which facilitates a holistic prediction on the regeneration outcome.

In contrast to VRP(natural), VRP(max) represents the best possible outcomes for recovering ecosystem functions, services, and biodiversity at scale, which can be attained either by accelerating through active intervention or by allowing for a longer period of natural regeneration under favorable conditions (Chazdon and Guariguata, 2016). As a theoretical assessment, VRP(max) is closely tied to the environmental constraints, allowing for estimation through a modelling approach based on environmental similarity (e.g., Bastin et al., 2019; Walker et al., 2022). This case study confirms the reliability of this approach and indicates its robust correlation at a finer scale. For instance, environmental factors explained 67% of the variance in VRP(max) in Hong Kong at a 30 m resolution, showing its sensitivity on fine-scale spatial heterogeneity. We found that precipitation emerges as a key driver determining VRP(max). This aligns with previous research highlighting its role in supporting ecosystem functioning and resilience (Ratcliffe et al., 2017). The marginal effect of the factors was shown using a partial dependence plot (Fig. A3), and the result indicates there exists a threshold (ca. 1100 mm of precipitation) where the VRP(max) increases significantly. Also, our results indicate that the mountainous regions exhibit a generally higher VRP(max) than the coastal areas. This could potentially be attributed to the water availability interacted by the rainwater storage capacity and groundwater supply in these respective areas. These analyses facilitate a deeper understanding on the drivers of the large variability in vegetation restoration potentials.

Finally, the restoration prioritization based on the integration of VRPs has successfully identified the hotspots with high restoration gains (Fig. 7). Yet, safeguarding these areas from fire remains a paramount concern, as these hotspot regions largely overlapped with areas of frequent fire occurrences (Chan et al., 2023). Despite the rapid pace of natural forest successional development in Hong Kong (Abbas et al., 2016), this process is significantly impeded by recurrent fires (Chan and Coomes, 2024). Moreover, the negative impact of fires on seed banks reduces the chance of natural regeneration in adjacent areas (Shi et al., 2022). Therefore, beyond the establishment of country parks, there may be a need for the government to intensify interventions in fire prevention policies and measures. Refinement is also needed to incorporate socioecological and political information with further stakeholder involvement at the appropriate intervention scale (Wortley et al., 2013).

4.3. Limitations and potential improvements

Our framework provides quantitative assessments on vegetation restoration potentials, which are useful for informing planning and

implementation to foster forest restoration at scale. Based on this case study and the implementation using local data, we have identified several considerations regarding the insights gained and potential limitations that need to be addressed. Firstly, the estimated VRP(max) may vary, as even when the forest reaches sufficient ages, climatic disturbances, background climate change, and other factors causing forest degradation may render VRP(max) unstable. Secondly, the timeframe of this study is limited. We focused on vegetation recovery potentials at the decadal scale primarily due to: 1) in response to the increasingly urgent Climate Action Plan (e.g., the 2050 carbon neutrality goal in Hong Kong), we aim to track the vegetation recovery trajectory on a decadal timescale so that the model can be used to inform potential outcomes in the near future; 2) we aim to minimize uncertainties arising from longer timescales, including anthropogenic disturbances (fires) and natural disasters (typhoons); and 3) from a feasibility aspect, it is difficult to cover the longer timeframe using the current data, i.e., the two-time LiDAR surveys which span a ten-year interval. As a result, when using “stable” regions as proxy patches to approximate the VRP(natural), the proxy patches may not encompass the ideal VRP(natural) and could potentially result in underestimation. This is because the “stable” regions were recognized based on the decade-span LiDAR data, while it is possible that these regions are still undergoing slow successional processes. In the case of Hong Kong, Abbas et al. observed a faster conversion from shrub to forest than from grassland to shrub, suggesting that there exists a lag, or bottleneck, in grassland invasion by woody vegetation (Abbas et al., 2016). In the absence of wildfires, shrubs and young trees typically replace grasslands within 10–15 years, and after another 15–30 years, they form secondary forests with a height of 10–16 m. Therefore, employing observations from a longer time series would enhance the accuracy of recovery potential estimations by improving the representativeness of the proxy patches.

There are also several aspects that deserve further investigation to refine this framework. One example is the vegetation recovery rate, which determines the time required for an ecosystem to return to an ideal state. Given the climate change scenario, the changes in light, temperature, rainfall, and atmospheric CO₂ concentration could generate impacts on plant phenology and physiology, and thus causing the change in recovery rate as well as the regeneration/restoration potential. This is especially evident by a few recent studies (e.g., Xu et al., 2023; Zhu et al., 2016). Additionally, while we have predicted the vegetation recovery potentials under ideal scenario, whether the environmental capacity can support additional trees still requires further mechanistic validation. For instance, whether groundwater resources can sustain the growth of a large number of trees (Christina et al., 2017). This could potentially be assessed in the future through physical process modeling. Furthermore, we may also take into account the climate events, such as intensified droughts, rising temperatures, extreme precipitations and their potential effects on vegetation growth, all of which can be integrated into the assessment of ecosystem recovery potentials.

5. Conclusion

In conclusion, this study developed a framework that integrates the natural regeneration potential and the maximum restoration potential into real-world ecosystem restoration planning at a finer spatial scale. This framework enables us to analyze the relationship between current vegetation status and vegetation recovery potentials, and accordingly we were able to determine different priority levels for restoration efforts. This information can assist policymakers in optimizing vegetation restoration options and promoting the protection and sustainable development of fragile ecosystems. Moving forward, this framework shows the potential to expand with multidimensional indicators to accommodate diverse research needs, such as carbon sequestration, biodiversity, and other ecosystem services. Restoration practices lie along a continuum rather than within discrete categories of natural versus active forms, and our framework facilitate their integration,

leading to a more practical and efficient restoration planning.

CRediT authorship contribution statement

He Zhang: Writing – original draft, Software, Methodology, Formal analysis, Data curation, Conceptualization. **Calvin K.F. Lee:** Writing – review & editing, Conceptualization. **Ying Ki Law:** Validation, Methodology, Data curation. **Aland H.Y. Chan:** Writing – review & editing, Validation, Data curation. **Jinlong Zhang:** Writing – review & editing. **Stephan W. Gale:** Writing – review & editing. **Alice Hughes:** Writing – review & editing. **Martha J. Ledger:** Writing – review & editing. **Man Sing Wong:** Writing – review & editing. **Amos P.K. Tai:** Writing – review & editing. **Billy C.H. Hau:** Writing – review & editing. **Jin Wu:** Writing – review & editing, Supervision, Funding acquisition, Conceptualization.

Declaration of competing interest

The authors declare the following financial interests/personal relationships which may be considered as potential competing interests: Jin Wu reports financial support was provided by National Natural Science Foundation of China. Jin Wu reports financial support was provided by HKU Seed Fund for Basic Research. Jin Wu reports financial support was provided by Hong Kong Research Grant Council Collaborative Research Fund. Jin Wu reports financial support was provided by The Hung Wing Physical Science Research Fund 2021-22. Jin Wu reports financial support was provided by The Innovation and Technology Fund (funding support to State Key Laboratories in Hong Kong of

Agrobiotechnology) of the HKSAR, China. Calvin K. F. Lee reports financial support was provided by the HKU 45th Round PDF Scheme. Ying Ki Law reports financial support was provided by the Research Grants Council of the Hong Kong SAR Government. If there are other authors, they declare that they have no known competing financial interests or personal relationships that could have appeared to influence the work reported in this paper.

Data availability

Data will be made available on request.

Acknowledgements

The work was supported by the National Natural Science Foundation of China (#31922090), HKU Seed Fund for Basic Research (#2021115931), Hong Kong Research Grant Council Collaborative Research Fund (#C5062-21GF), the Hung Ying Physical Science Research Fund 2021-22, HKU Science Faculty RAE Improvement Fund 2023-24, and the Innovation and Technology Fund (funding support to State Key Laboratories in Hong Kong of Agrobiotechnology) of the HKSAR, China. C.K.F. Lee was also in part supported by the HKU 45th Round PDF Scheme. Y. Law and B. Hau were supported by the Centre for Slope Safety (AoE/E-603/18) of the Research Grants Council of the Hong Kong SAR Government. We thank Civil Engineering and Development Department (CEDD) of HKSAR provides the open-sourced landslide inventory records, and Lands department of HKSAR provides historical aerial photographs in public use.

Appendix

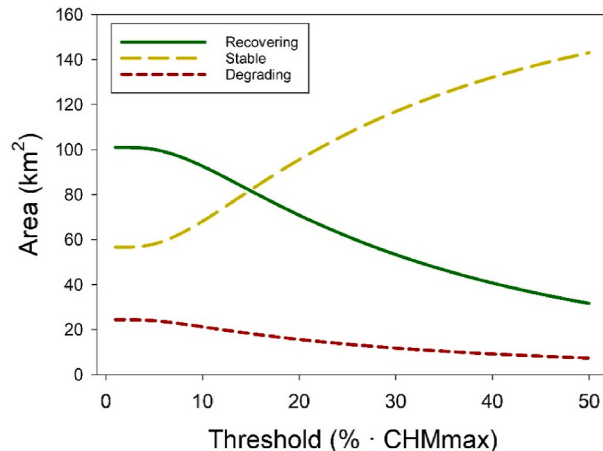


Fig. A1. Varying threshold for determining the vegetation recovery status (recovering, degrading and stable) using canopy height information.

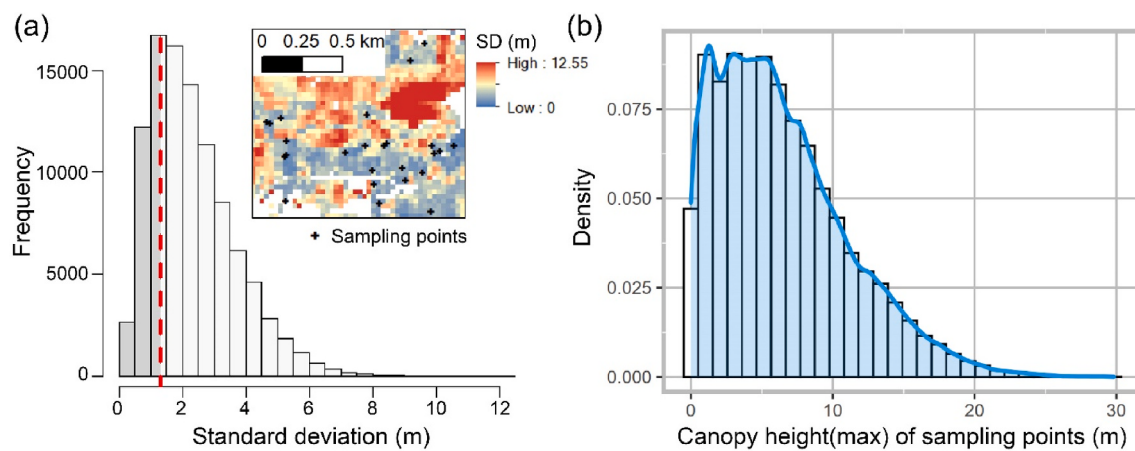


Fig. A2. (a) Standard deviation (SD) distribution of maximum canopy heights under different sliding window sizes. When taking 1st quartile of the sorted SD as threshold, the distribution of sample points is shown in the example map. (b) The distribution of the maximum vegetation heights corresponding to the aforementioned sampling points.

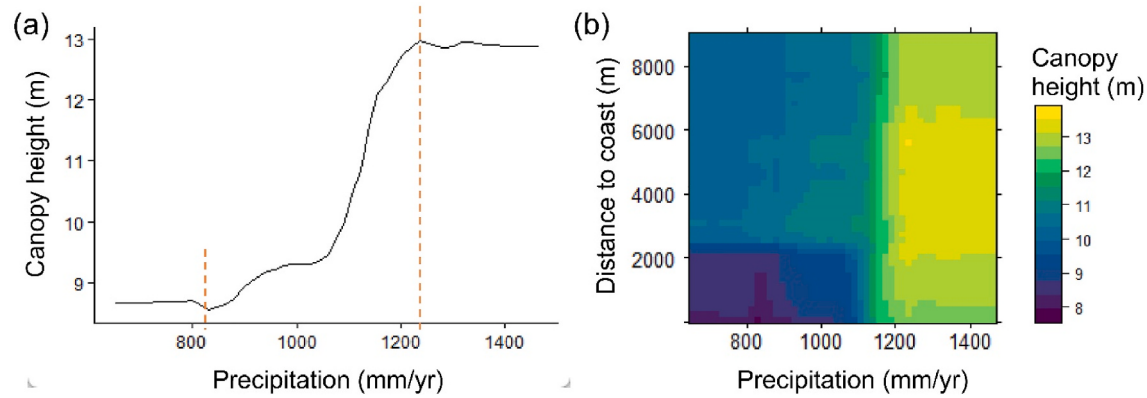


Fig. A3. Partial dependence plots showing the relationship between important variables in the random forest model (precipitation of warmest quarter and distance to coast) and the predicted outcome (potential canopy height) while holding other variables constant. (a) relationship between precipitation of warmest quarter and potential canopy height (b) relationship between precipitation of warmest quarter, distance to coast and potential canopy height.

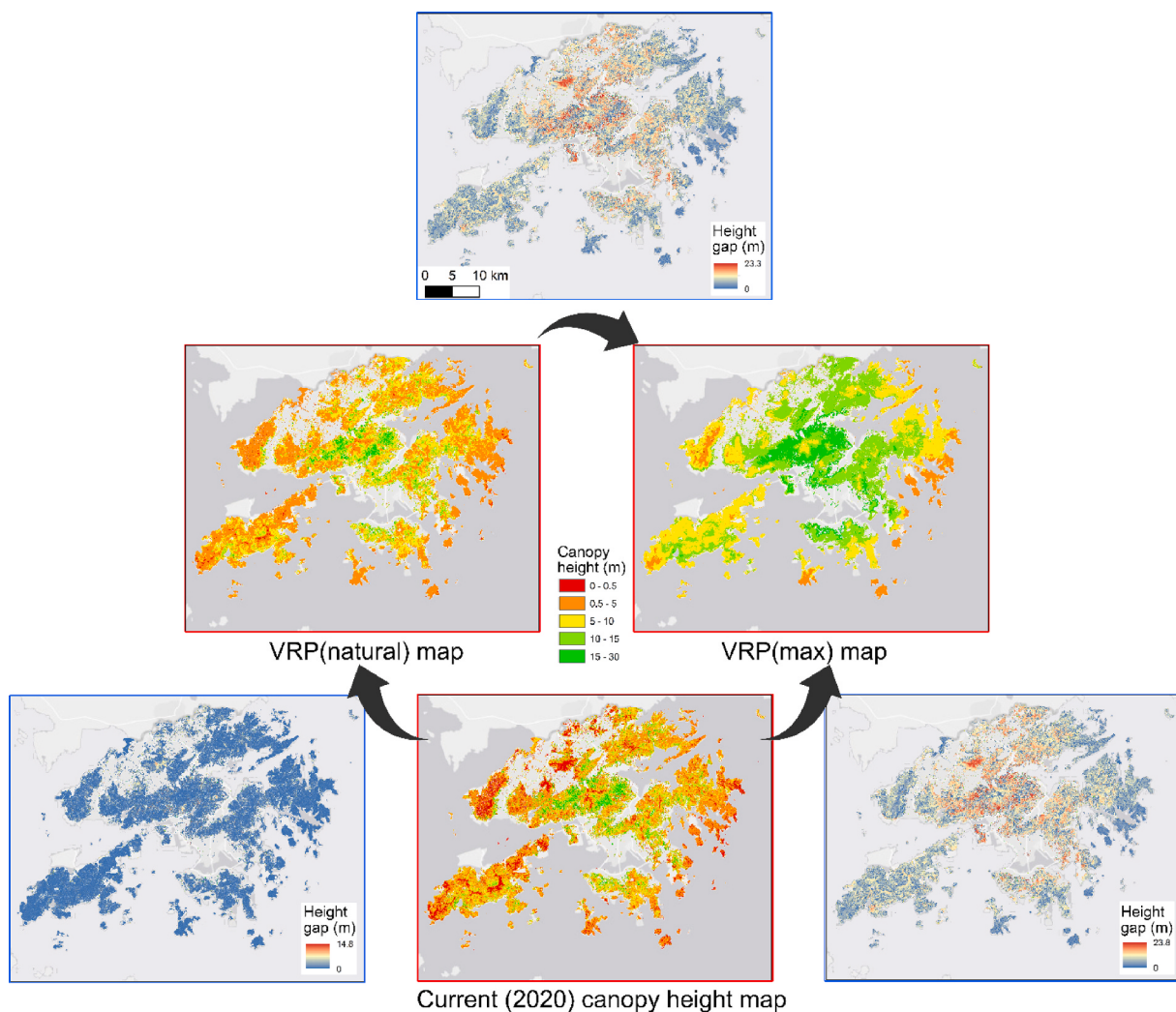


Fig. A4. The current canopy height map and VRP maps in Hong Kong region (in red frame), and height gap maps between each pair of categories (in blue frame).

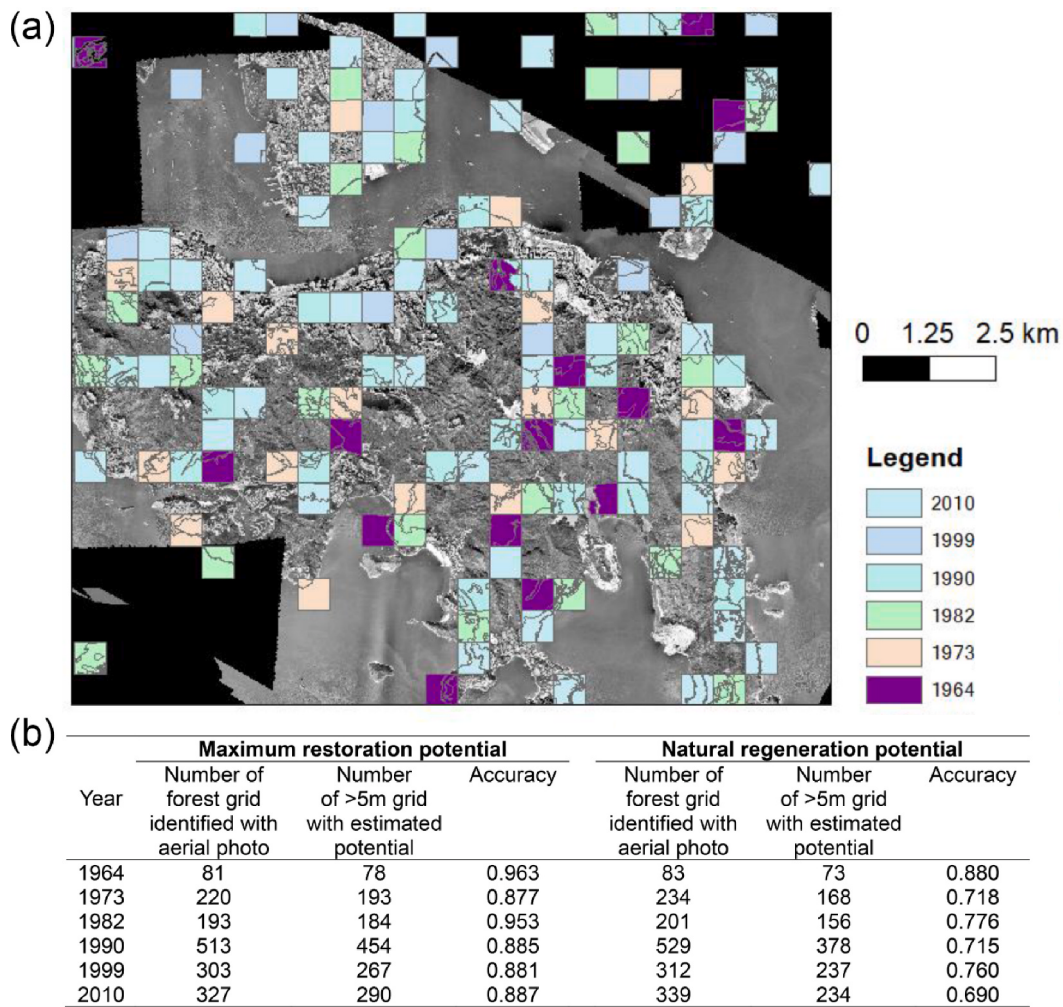


Fig. A5. Results of external validation using historical aerial photos. (a) Demonstration of external validation where the land classification was made by visual interpretation. (b) Summary of results using 5 m as threshold to match with forest land cover.

Table A1

Description of environmental variables used for predicting maximum restoration potential in the random forest model.

Description	Unit	5%	50%	95%	Filename
Aspect (Northness)	index	-0.99	0	0.99	aspect.tif
Aspect (Degree)	°	18	180	341	aspect_degree.tif
Slope	°	0	17	33	slope.tif
Terrain Roughness	index	0.33	24.95	50.67	rough.tif
Elevation	m	5	84	407	elevation.tif
Aspect * Slope	index	-23.5	0	23.58	aspect_x_slope.tif
Distance to Coast	m	68	1349	6186	waterdist.tif
Relative Elevation (60 m radius)	m	0	16	37	relelev60.tif
Relative Elevation (120 m radius)	m	0	28	69	relelev120.tif
Relative Elevation (240 m radius)	m	2	46	124	relelev240.tif
Relative Elevation (480 m radius)	m	2	64	208	relelev480.tif
Relative Elevation (960 m radius)	m	3	76	308	relelev960.tif
Water Proximity (0.75 km radius)	proportion	0.52	1	1	water25.tif
Water Proximity (1.5 km radius)	proportion	0.4	0.98	1	water50.tif
Water Proximity (3 km radius)	proportion	0.33	0.88	1	water100.tif
Water Proximity (6 km radius)	proportion	0.31	0.74	1	water200.tif
Water Proximity (12 km radius)	proportion	0.27	0.66	0.94	water400.tif
Annual Mean Temperature	°C	20.8	22.9	24	biovars_t_1.tif
Mean Diurnal Range (Mean (max temp-min temp))	°C	4.9	6.2	7.7	biovars_t_2.tif
Isothermality (bio2/bio7) (* 100)	index	27.4	31.9	35.6	biovars_t_3.tif
Temperature Seasonality (standard deviation * 100)	index	467	496	512	biovars_t_4.tif
Average High Temperature of Warmest Month	°C	28.9	31.5	32.8	biovars_t_5.tif
Average Low Temperature of Coldest Month	°C	9.5	11.7	13.9	biovars_t_6.tif
Temperature Annual Range (bio5-bio6)	°C	17.7	19.6	21.6	biovars_t_7.tif
Mean Temperature of Wettest Quarter	°C	25.8	27.8	29.2	biovars_t_8.tif

(continued on next page)

Table A1 (continued)

Description	Unit	5%	50%	95%	Filename
Mean Temperature of Driest Quarter	°C	14.4	16.3	17.4	biovars_t_9.tif
Mean Temperature of Warmest Quarter	°C	25.9	28.2	29.2	biovars_t_10.tif
Mean Temperature of Coldest Quarter	°C	14.4	16.3	17.4	biovars_t_11.tif
Annual Precipitation	mm	1738	2079	2415	biovars_t_12.tif
Precipitation of Wettest Month	mm	345	425	521	biovars_t_13.tif
Precipitation of Driest Month	mm	25	32	35	biovars_t_14.tif
Precipitation Seasonality (Coefficient of Variation)	index	78.7	82.8	86	biovars_t_15.tif
Precipitation of Wettest Quarter	mm	883	1085	1276	biovars_t_16.tif
Precipitation of Driest Quarter	mm	86	104	112	biovars_t_17.tif
Precipitation of Warmest Quarter	mm	814	1054	1260	biovars_t_18.tif
Precipitation of Coldest Quarter	mm	86	104	112	biovars_t_19.tif
Extreme Temperature Annual Range	°C	26.3	29	32.1	avars_annual_range.tif
Annual Mean Dew Point	°C	17.3	18.4	19.1	avars_dewp_mean.tif
Annual Mean Relative Humidity	%	75.4	80.4	84.9	avars_humid_mean.tif
Maximum Temperature of Warmest Month	°C	32.3	35	36.2	avars_max_tmax.tif
Minimum Temperature of Coldest Month	°C	2.4	5.6	8.6	avars_min_tmin.tif
Annual Mean Air Pressure	hPa	1012.5	1012.8	1013.4	avars_press_mean.tif
Actual Annual Mean Temperature	°C	20.3	22.4	23.6	avars_tmean_mean.tif
Annual Mean Wind Speed	km/h	5.4	11.6	19.2	avars_windsp_mean.tif
Urbanicity (sigma = 10)	%	0	0	68.9	urbanicity_gauss10.tif
Urbanicity (sigma = 50)	%	0	1.5	56	urbanicity_gauss50.tif
Urbanicity (sigma = 100)	%	0	3.3	50.1	urbanicity_gauss100.tif
Soil CEC content	mmol/kg	30–60	60–100	>140	soil_map3.tif
Soil organic carbon content	%	0.51–1	1.01–2	2.01–2.5	soil_map4.tif
Soil total nitrogen content	mg/kg	50–100	100–150	>200	soil_map5.tif
Soil total phosphorus content	mg/kg	50–100	100–200	>500	soil_map6.tif

References

- Abbas, S., Nichol, J.E., Fischer, G.A., 2016. A 70-year perspective on tropical forest regeneration. *Sci. Total Environ.* 544, 544–552. <https://doi.org/10.1016/j.scitotenv.2015.11.171>.
- Arroyo-Rodríguez, V., Melo, F.P., Martínez-Ramos, M., Bongers, F., Chazdon, R.L., Meave, J.A., Norden, N., Santos, B.A., Leal, I.R., Tabarelli, M., 2017. Multiple successional pathways in human-modified tropical landscapes: new insights from forest succession, forest fragmentation and landscape ecology research. *Biol. Rev.* 92 (1), 326–340.
- Ashton, M.S., Gunatilleke, C.V.S., Gunatilleke, I., Singhakumara, B.M.P., Gamage, S., Shibayama, T., Tomimura, C., 2014. Restoration of rain forest beneath pine plantations: a relay floristic model with special application to tropical South Asia. *For. Ecol. Manag.* 329, 351–359.
- Bastin, J.F., Finegold, Y., Garcia, C., Mollicone, D., Rezende, M., Routh, D., Zohner, C.M., Crowther, T.W., 2019. The global tree restoration potential. *Science* 364 (6448), 76–79. <https://doi.org/10.1126/science.aax0848>.
- Cazzolla Gatti, R., Di Paola, A., Bombelli, A., Noce, S., Valentini, R., 2017. Exploring the relationship between canopy height and terrestrial plant diversity. *Plant Ecol.* 218, 899–908.
- Chan, A.H.Y., Coomes, D.A., 2024. Fire traps in the wet subtropics: new perspectives from Hong Kong. *J. Appl. Ecol.* 1365–2664, 14575 <https://doi.org/10.1111/1365-2664.14575>.
- Chan, A.H.Y., Guizar-Coutiño, A., Kalamandeen, M., Coomes, D.A., 2023. Reconstructing 34 Years of fire history in the wet, subtropical vegetation of Hong Kong using Landsat. *Rem. Sens.* 15 (6), 1489. <https://doi.org/10.3390/rs15061489>.
- Chazdon, R.L., 2013. Making tropical succession and landscape reforestation successful. *J. Sustain. For.* 32 (7), 649–658.
- Chazdon, R.L., Falk, D.A., Banin, L.F., Wagner, M., J Wilson, S., Grabowski, R.C., Suding, K.N., 2021. The intervention continuum in restoration ecology: rethinking the active-passive dichotomy. *Restor. Ecol.*, e13535 <https://doi.org/10.1111/rec.13535>.
- Chazdon, R.L., Guariguata, M.R., 2016. Natural regeneration as a tool for large-scale forest restoration in the tropics: prospects and challenges. *Biotropica* 48 (6), 716–730. <https://doi.org/10.1111/btp.12381>.
- Chazdon, R.L., Lindenmayer, D., Guariguata, M.R., Crouzeilles, R., Rey Benayas, J.M., Lazos Chávero, E., 2020. Fostering natural forest regeneration on former agricultural land through economic and policy interventions. *Environ. Res. Lett.* 15 (4), 043002 <https://doi.org/10.1088/1748-9326/ab79e6>.
- Chazdon, R.L., Uriarte, M., 2016. Natural regeneration in the context of large-scale forest and landscape restoration in the tropics. *Biotropica* 48 (6), 709–715.
- Choi, C., Shi, X., Shi, J., Gan, X., Wen, C., Zhang, J., Jackson, M.V., Fuller, R.A., Gibson, L., 2022. China's Ecological Conservation Redline policy is a new opportunity to meet post-2020 protected area targets. *Conservation Letters* 15 (2), e12853.
- Christina, M., Nouvellon, Y., Laclau, J.P., Stape, J.L., Bouillet, J.P., Lambais, G.R., le Maire, G., 2017. Importance of deep water uptake in tropical eucalypt forest. *Funct. Ecol.* 31 (2), 509–519. <https://doi.org/10.1111/1365-2435.12727>.
- Cook-Patton, S.C., Leavitt, S.M., Gibbs, D., Harris, N.L., Lister, K., Anderson-Teixeira, K.J., Briggs, R.D., Chazdon, R.L., Crowther, T.W., Ellis, P.W., Griscom, H.P.,
- Herrmann, V., Holl, K.D., Houghton, R.A., Larrosa, C., Lomax, G., Lucas, R., Madsen, P., Malhi, Y., et al., 2020. Mapping carbon accumulation potential from global natural forest regrowth. *Nature* 585 (7826), 545–550. <https://doi.org/10.1038/s41586-020-2686-x>.
- Cressie, N., 1990. The origins of kriging. *Math. Geol.* 22, 239–252.
- Crouzeilles, R., Beyer, H.L., Monteiro, L.M., Feltran-Barbieri, R., Pessôa, A.C.M., Barros, F.S.M., Lindenmayer, D.B., Lino, E.D.S.M., Grelle, C.E.V., Chazdon, R.L., Matsumoto, M., Rosa, M., Latawiec, A.E., Strassburg, B.B.N., 2020. Achieving cost-effective landscape-scale forest restoration through targeted natural regeneration. *Conservation Letters* 13 (3), e12709. <https://doi.org/10.1111/conl.12709>.
- Crouzeilles, R., Ferreira, M.S., Chazdon, R.L., Lindenmayer, D.B., Sansevero, J.B.B., Monteiro, L., Iribarren, A., Latawiec, A.E., Strassburg, B.B.N., 2017. Ecological restoration success is higher for natural regeneration than for active restoration in tropical forests. *Sci. Adv.* 3 (11), e1701345.
- Dormann, C.F., Elith, J., Bacher, S., Buchmann, C., Carl, G., Carré, G., Marquéz, J.R.G., Gruber, B., Lafourcade, B., Leitão, P.J., 2013. Collinearity: a review of methods to deal with it and a simulation study evaluating their performance. *Ecography* 36 (1), 27–46.
- European Commission, 2019. Communication from the commission to the European parliament, the European Council, the Council, the European economic and social committee and the committee of the regions—the European green deal. Document 52019DC0640 640.
- Feng, X., Fu, B., Piao, S., Wang, S., Caias, P., Zeng, Z., Lü, Y., Zeng, Y., Li, Y., Jiang, X., Wu, B., 2016. Revegetation in China's Loess Plateau is approaching sustainable water resource limits. *Nat. Clim. Change* 6 (11), 1019–1022. <https://doi.org/10.1038/nclimate3092>.
- Gamfeldt, L., Snäll, T., Bagchi, R., Jonsson, M., Gustafsson, L., Kjellander, P., Ruiz-Jaen, M.C., Fröberg, M., Stendahl, J., Philipson, C.D., Mikusiński, G., Andersson, E., Westerlund, B., Andrén, H., Moberg, F., Moen, J., Bengtsson, J., 2013. Higher levels of multiple ecosystem services are found in forests with more tree species. *Nat. Commun.* 4 <https://doi.org/10.1038/ncomms2328>.
- Greenwell, B.M., 2017. pdp: an R package for constructing partial dependence plots. *R J* 9 (1), 421.
- Gribov, A., Krivoruchko, K., Ver Hoef, J., 2006. Modeling the Semivariogram: New Approach, Methods Comparison, and Simulation Study.
- Griscom, B.W., Adams, J., Ellis, P.W., Houghton, R.A., Lomax, G., Miteva, D.A., Schlesinger, W.H., Shoch, D., Siikamäki, J.V., Smith, P., 2017. Natural climate solutions. *Proc. Natl. Acad. Sci. USA* 114 (44), 11645–11650.
- Griscom, B.W., Busch, J., Cook-Patton, S.C., Ellis, P.W., Funk, J., Leavitt, S.M., Lomax, G., Turner, W.R., Chapman, M., Engelmann, J., 2020. National mitigation potential from natural climate solutions in the tropics. *Philosophical Transactions of the Royal Society B* 375 (1794), 20190126.
- Heydel, F., Cunze, S., Bernhardt-Römermann, M., Tackenberg, O., 2014. Long-distance seed dispersal by wind: disentangling the effects of species traits, vegetation types, vertical turbulence and wind speed. *Ecol. Res.* 29 (4), 641–651. <https://doi.org/10.1007/s11284-014-1142-5>.
- Isenburg, M., 2020. LAStools—Efficient LiDAR Processing Software. academic license version 200509.

- Jiang, X., Ziegler, A.D., Liang, S., Wang, D., Zeng, Z., 2022. Forest restoration potential in China: implications for carbon capture. *Journal of Remote Sensing* 2022, 1–13. <https://doi.org/10.34133/remotesensing.0006>.
- Lewis, S.L., Wheeler, C.E., Mitchell, E.T.A., Koch, A., 2019. Restoring natural forests is the best way to remove atmospheric carbon. *Nature* 568 (7750), 25–28.
- Luo, Y., Li, Z., Wu, L., Wu, S., Zhang, G., Zhou, S., Zhao, Y., Zhao, Q., Huang, M., Zhang, H., 2007. Hong Kong Soils and Environment. 科学出版社. <https://books.google.com.hk/books?id=ivzLMQAACAAJ>.
- Mansourian, S., Berrahmouni, N., 2021. Review of Forest and Landscape Restoration in Africa 2021. Food & Agriculture Org.
- Masson-Delmotte, V., Zhai, P., Pörtner, H.-O., Roberts, D., Skea, J., Shukla, P.R., Pirani, A., Moufouma-Okia, W., Péan, C., Pidcock, R., Connors, S., Matthews, J.B.R., Chen, Y., Zhou, X., Gomis, M.I., Lonnoy, E., Maycock, T., Tignor, M., Waterfield, T. IPCC, 2018. Global Warming of 1.5 °C. An IPCC Special Report on the Impacts of Global Warming of 1.5 °C above Pre-Industrial Levels and Related Global Greenhouse Gas Emission Pathways, in the Context of Strengthening the Global Response to the Threat of Climate Change. Sustainable Development, and Efforts to Eradicate Poverty.
- Meng, X., Pi, H., Gao, X., He, P., Lei, J., 2023. A high-accuracy vegetation restoration potential mapping model integrating similar habitat and machine learning. *Land Degrad. Dev.* 34 (4), 1208–1224.
- Messinger, J., Winterbottom, B., 2016. African forest landscape restoration initiative (AFR100): restoring 100 million hectares of degraded and deforested land in Africa. *Nature & Faune* 30 (2), 14–17.
- Moreno-Mateos, D., Barbier, E.B., Jones, P.C., Jones, H.P., Aronson, J., López-López, J.A., McCrackin, M.L., Meli, P., Montoya, D., Rey Benayas, J.M., 2017. Anthropogenic ecosystem disturbance and the recovery debt. *Nat. Commun.* 8, 8–13. <https://doi.org/10.1038/ncomms14163>.
- Morgan, B., Guénard, B., 2018. Local models reveal greater spatial variation than global grids in an urban mosaic: Hong Kong climate, vegetation, and topography rasters. *Local Models Reveal Greater Spatial Variation than Global Grids in an Urban Mosaic: Hong Kong Climate, Vegetation, and Topography Rasters* 1–26.
- Morgan, B., Guénard, B., 2019. New 30 m resolution Hong Kong climate, vegetation, and topography rasters indicate greater spatial variation than global grids within an urban mosaic. *Earth Syst. Sci. Data* 11 (3), 1083–1098.
- Pereira, H.M., Ferrier, S., Walters, M., Geller, G.N., Jongman, R.H., Scholes, R.J., Bruford, M.W., Brummitt, N., Butchart, S.H., Cardoso, A., 2013. Essential biodiversity variables. *Science* 339 (6117), 277–278.
- Phillips, L.B., Hansen, A.J., Flather, C.H., 2008. Evaluating the species energy relationship with the newest measures of ecosystem energy: NDVI versus MODIS primary production. *Remote Sensing of Environment* 112 (12), 4381–4392.
- Poorter, L., Bongers, F., Aide, T.M., Almeyda Zambrano, A.M., Balvanera, P., Becknell, J. M., Boukili, V., Brancalion, P.H.S., Broadbent, E.N., Chazdon, R.L., 2016. Biomass resilience of Neotropical secondary forests. *Nature* 530 (7589), 211–214.
- Potapov, P., Hansen, M.C., Pickens, A., Hernandez-Serna, A., Tyukavina, A., Turubanova, S., Zalas, V., Li, X., Khan, A., Stolle, F., 2022. The global 2000–2020 land cover and land use change dataset derived from the Landsat archive: first results. *Frontiers in Remote Sensing* 3, 856903.
- Ratcliffe, S., Wirth, C., Jucker, T., van Der Plas, F., Scherer-Lorenzen, M., Verheyen, K., Allan, E., Benavides, R., Bruehlheide, H., Ohse, B., 2017. Biodiversity and ecosystem functioning relations in European forests depend on environmental context. *Ecol. Lett.* 20 (11), 1414–1426.
- Reid, J.L., Fagan, M.E., Zahawi, R.A., 2018. Positive site selection bias in meta-analyses comparing natural regeneration to active forest restoration. *Sci. Adv.* 4 (5), eaas9143.
- Shi, Y.-F., Shi, S.-H., Jiang, Y.-S., Liu, J., 2022. A global synthesis of fire effects on soil seed banks. *Global Ecology and Conservation* 36, e02132.
- Summit, U.N.C., 2014. New York Declaration on Forests. United Nations, New York, NY.
- Torrubia, S., McRae, B.H., Lawler, J.J., Hall, S.A., Halabisky, M., Langdon, J., Case, M., 2014. Getting the most connectivity per conservation dollar. *Front. Ecol. Environ.* 12 (9), 491–497.
- van Iersel, W., Straatsma, M., Addink, E., Middelkoop, H., 2018. Monitoring height and greenness of non-woody floodplain vegetation with UAV time series. *ISPRS J. Photogrammetry Remote Sens.* 141, 112–123.
- Walker, W.S., Gorelik, S.R., Cook-Patton, S.C., Baccini, A., Farina, M.K., Solvik, K.K., Ellis, P.W., Sanderman, J., Houghton, R.A., Leavitt, S.M., Schwalm, C.R., Griscom, B. W., 2022. The global potential for increased storage of carbon on land. *Proceedings of the National Academy of Sciences of the United States of America* 119 (23), 1–12. <https://doi.org/10.1073/pnas.2111312119>.
- Wortley, L., Hero, J., Howes, M., 2013. Evaluating ecological restoration success: a review of the literature. *Restor. Ecol.* 21 (5), 537–543.
- Xu, H., Yue, C., Zhang, Y., Liu, D., Piao, S., 2023. Forestation at the right time with the right species can generate persistent carbon benefits in China. *Proc. Natl. Acad. Sci. USA* 120 (41), e2304988120.
- Zahawi, R.A., Holl, K.D., Cole, R.J., Reid, J.L., 2013. Testing applied nucleation as a strategy to facilitate tropical forest recovery. *J. Appl. Ecol.* 50 (1), 88–96.
- Zhao, X., Guo, Q., Su, Y., Xue, B., 2016. Improved progressive TIN densification filtering algorithm for airborne LiDAR data in forested areas. *ISPRS J. Photogrammetry Remote Sens.* 117, 79–91.
- Zhu, H., Zhang, J., Cheuk, M.L., Hau, B.C., Fischer, G.A., Gale, S.W., 2023. Monoculture plantations impede forest recovery: evidence from the regeneration of lowland subtropical forest in Hong Kong. *Frontiers in Forests and Global Change* 6, 1098666.
- Zhu, Z., Piao, S., Myneni, R.B., Huang, M., Zeng, Z., Canadell, J.G., Ciais, P., Sitch, S., Friedlingstein, P., Arneth, A., 2016. Greening of the earth and its drivers. *Nat. Clim. Change* 6 (8), 791–795.
- Zhuang, X.Y., Gorlett, R.T., 1997. Forest and forest succession in Hong Kong, China. *J. Trop. Ecol.* 13 (6), 857–866.
- Zuo, Z., Dong, L., Knyazikhin, Y., Myneni, R.B., 2023. Simulating potential tree height for beech–maple–birch forests in northeastern United States on google earth engine. *Journal of Remote Sensing* 3, 84. <https://doi.org/10.34133/remotesensing.0084>.